MCAT Institute
Final Report
93-07

TURBULENCE MODELING FOR HYPERSONIC FLIGHT

Jorge E. Bardina

February 1993

NCC2-585

MCAT Institute
3933 Blue Gum Drive
San Jose, CA 95127

NCC 2-585

ANNUAL REPORT

Technical Proposal

The objective of the proposed work is to continue the work to develop, verify and incorporate the baseline two-equation turbulence models which account for the effects of compressibility at high speeds into a three-dimensional Reynolds averaged Navier-Stokes (**RANS**) code and to provide documented descriptions of the models and their numerical procedures so that they can be implemented into the NASP CFD codes.

Computational Fluid Dynamics (**CFD**) is recognized as a significant engineering design tool in modern hypersonic projects such as the National Aerospace Plane (**NASP**). The design of the NASP vehicle is a highly complex process. One of the critical tasks involved in such a process is the ability of the turbulence model to predict hypersonic viscous/inviscid interactions, mixing problems, transition, chemical nonequilibria, and a range of other turbulence phenomena.

Turbulence models are developed on the basis of insight gained from experimental and theoretical research. The complexity of turbulence requires that the mathematical models be guided by the flow physics in a rational and practical approach. Test and validation of new models with data of recognized quality is an essential step toward model acceptability. A database with a detailed experimental information on high speed turbulent flows is currently being completed. This database provides a benchmark for testing and validation of the compressible model modifications. Specific topics for the database are

shock wave/boundary layer interactions, high-speed attached boundary layers with pressure gradients, and supersonic shear layer mixing.

The baseline $k-\omega$ and $k-\epsilon$ models with the proposed length-scale and rapid compression modifications have already been implemented into the 3-D Navier-Stokes base code. The turbulence models have been tested against experimental data of the hypersonic database collection. The validation ranges from simple flat plate flows to complex 3-D flows. They included theoretical correlations, Mach 5 supersonic flat plate turbulent flow, Mach 3 supersonic compression corner with flow separation, and Mach 8 hypersonic 3-D shock-wave boundary layer interaction flows generated with single fins and two oblique fins mounted on a flat plate surface. A major consideration throughout the research effort will continue to be the development of improved compressibility corrections to the turbulence models and the identification of models which are superior in their predictive capabilities.

Work Statement

The following is the work statement proposed to be accomplished within this past research year:

1. Incorporate $k - \epsilon$ models into base code and evaluate performance against 2-D compressible turbulent flows (Mach 5 flat plate flow and Mach 3 compression ramp).
2. Test and evaluate improved numerics that take into account second law of thermodynamics and higher-order TVD flux limiters.
3. Study and continue development of compressibility corrections for 3-D turbulence models (numerical simulations of 3-D shock wave / boundary layer interaction (SWBLI) at $M_\infty = 8.2$).
4. Supervise and deliver information needed to implement compressible two-equation turbulence models into 3-D codes.

Work Accomplished

1. The baseline turbulence models have been incorporated into the base **RANS** 3-D Reynolds Averaged Navier-Stokes code and validated against the Mach 5 flat plate boundary layer flow and the 2-D codes of T.J. Coakley and P.G. Huang. The two equation turbulence models already implemented are:
   - Wilcox $k-\omega$ model (baseline model)
   - Wilcox transition $k-\omega$ model
   - Jones-Launder $k-\epsilon$ model
   - Launder-Sharma $k-\epsilon$ model (baseline model)
   - Chien $k-\epsilon$ model
2. Four important model modifications have been implemented and subject to different database tests:
   - A length scale modification in order to decrease the heat transfer rate in flow reattachment zones (all models).
   - A rapid compression modification to increase the size of the flow separation zone in high speed flows (all models).
   - A rotation or vortex stretching length scale modification to decrease the level of turbulent dissipation in flow recirculating zones (all models).
   - A turbulence transition modification to simulate flow transition and complex surfaces with both laminar and turbulent compressible flow zones ($k-\omega$ model).
3. Numerical simulations with and without the different combinations of model modifications have been done. These simulations have been based on the following flows:
   - Mach 14 laminar boundary layer on a 24° compression ramp

(code validation).

- Mach 5 flat plate turbulent boundary layer (turbulence modeling validation).
- Mach 3 separated turbulent boundary layer on a 24° compression ramp (turbulent flow separation validation).
- Mach 8 shock wave / turbulent boundary layer interaction generated with a 15° and a 10° fin mounted on a cooled flat plate with $T_{wall}/T_\infty = 0.3$ and $Re_\infty = 5 \cdot 10^6$ (complex 3-D SWBLI with crossflow separation).
- Mach 8 intersecting shock waves / turbulent boundary layer interaction generated with two 15° fins mounted on a flat plate (complex 3-D SWBLI with completely crossflow separation).

4. Important results:
   - The baseline models provide excellent agreement with the experimental data in the prediction of the pressure profiles, skin friction, and heat transfer rate on the cooled flat plate of the complex 3-D SWBLI flow at Mach 8.
   - The baseline models provide good agreement with the experimental measurements of pitot pressure in the crossflow zone of the 3-D SWBLI.
   - The length scale and rapid compression modifications do not improve the prediction of the effects of crossflow separation. Although, they have been shown to significantly improve the predictions of 2-D hypersonic separated flows.
   - The standard models provide good agreement with experimental measurements of flow separation in the Mach 3 supersonic flow (24° compression ramp). However, they underpredict the

size of flow separation in hypersonic flows at $M_\infty = 7$ and $M_\infty = 9$ (P.G. Huang and T.J. Coakley) and transonic flows (F. Menter).

- The rotation modification together with the length scale and rapid compression modifications improve the prediction of flow separation, while the length scale and rapid compression modifications overpredict the size of flow separation in the Mach 3 supersonic flow.
- The models do not have the capability to predict the heat transfer rate and the skin friction on the laminar fin with a turbulent boundary layer on its junction with the flat plate. All the models overpredict the experimental measurements. This is a weakness of the present models that we plan to analyze.
- The low Reynolds number transition modification proposed by Dr. David Wilcox improves the agreement with experimental data on transition Reynolds number in the Mach 5 flat plate boundary layer. It predicts poorly the heat transfer rate on the fin surface (turbulent / laminar boundary layer) of the 3-D SWBLI flow.
- The transition Reynolds number is very sensitive to the inflow turbulence levels and the free stream turbulence. The model is also very sensitive to freestream turbulent kinetic energy (Dr. Thomas Coakley). Parallel research has shown that small values of free stream specific dissipation rate ω has strong influence in the prediction of turbulent free shear flows and weaker influence in the prediction of attached boundary layers (F. Menter).

5. Improved numerics have been tested and implemented into the 3-D **RANS** Code.
   - Different higher-order finite difference numerics and TVD flux limiters methods have been studied and developed for the numerical method of the turbulence equations and the Reynolds-Averaged Navier-Stokes equations.
   - This research has shown that there are unlimited number of averaging procedures for flux-difference splitting methods that are consistent with Roe's conservative property U. In general, the Jacobian matrix of the discrete system is composed of a particular solution and an homogeneous solution. Roe's geometric averaging procedure represents one of these solutions, while the arithmetic averaging procedure incorporated in the **RANS3D** code represents another solution. All these methods are consistent in their limit with the Jacobian matrix of the continuos system.
   - The second-order flux limiters and the flux-difference splitting based on arithmetic averaging have been improved and tested in the simulation of the $M = 14.1$ laminar hypersonic 24° ramp and the turbulent flow at $M = 5$ on the cooled flat plate. The results are consistent with previous simulations and the running time improved 18%.
   - The code has been improved in user friendliness with a general input subroutine that reads the input data (parameters of turbulence models, different implicit boundary approximations in each direction, etc..), instead of using an specific code for each case (such as the **CNS** code).

- The 3-D code has been delivered to Dr. Florian Menter (Modeling and Experimental Validation Branch) in order to study the ability of the turbulence models and modifications to predict transonic flows. It has been requested by Dr. Ethiraj Venkatapathy (Aerothermodynamics Branch) in order to study shock waves / turbulent boundary layer interactions in inlets. It has been requested by McDonnell Douglas Space Systems Company to study high-speed turbulence aero-optics.
- Plotting programs for the 3-D simulations based on **PV-WAVE** coupled with **FRAME** software have been developed. These programs reduce and plot different combinations of mean variables and turbulence statistics.
- The numerical simulations have been run with the Cray-YMP and the Cray-2 NAS computers at NASA Ames Research Center.

6. A paper[1] has been written and presented with different results of the 3-D Navier-Stokes simulations in the AIAA Fourth International Aerospace Planes Conference held on December 1992 in Orlando, Florida. The paper is titled "Two-Equation Turbulence Modeling for 3-D Hypersonic Flows," and co-authored with T.J. Coakley and J.G. Marvin. The organizer of the Meeting session was Dr. John Hicks, NASP Chief Engineer.

Future Work

1. Develop a theoretical study of the improved compressibility corrections to the turbulence models in the boundary layer equations to identify their superior predictive capabilities. Present models do not support the 'production equals dissipation' balance in high speed flows. The model equations need to be analyzed by wall zone layers with appropriate boundary interface of the nonlinear equations.
2. Test and evaluate refinements of the baseline two-equation turbulence models implemented in the previous phase. Research focused in compressibility corrections for flow separation, transition, and low Reynolds number coefficients in wall sublayers.

   Incorporate the following low Reynolds number modifications into base code[2-4]:

   - Huang-Coakley $k-\epsilon$ model.
   - So-Zhang-Speziale $k-\epsilon$ model.
   - Coakley $q-\omega$ model.
   - Menter $k-\omega/k-\epsilon$ model.
   - Rodi $k-\epsilon$ with one equation model in sublayer zone.

   Validate the turbulence models against experimental data of the following flows[5]:

   - Mach 5 flat plate flow.
   - Mach 3 compression corner flow.
   - Mach 9 compression corner flow.
   - Mach 7 cylinder-flare flow.
3. Study and development of baseline modifications for 3-D turbulence

flows:

3a. Simulate 3-D SWBLI (1 fin), $M_\infty = 8.2$, of M.I. Kussoy and K.C. Horstman[6].

3b. Simulate 3-D intersecting SWBLI (2 fins), $M_\infty = 8.3$, of M.I. Kussoy and K.C. Horstman[7].

3c. Simulate 3-D intersecting SWBLI (2 fins), $M_\infty = 4$, of T.J. Garrison and G.S. Settles[8].

3d. Simulate 3-D intersecting SWBLI (2 oblique fins), $M_\infty = 8.3$, of Bahrami, P. et al[9].

3e. Simulate 3-D intersecting SWBLI (2 fins with top wall), $M_\infty = 8.3$, of M.I. Kussoy and C.C. Horstman[10].

4. Documentation. Supervise and deliver information needed to use the 3-D **RANS** code, to implement the baseline turbulence models into the **NASP** 3-D codes, and to documented descriptions of the models and their numerical procedures so that they can be implemented into the NASP CFD codes.

5. 3-D Navier-Stokes code. Improve code with self adjusting parameters to run multiple 3-D grids with multiple segments and multiple boxes. main effort to simulate flows with complex physics to improve understanding of the turbulence effects.

Acknowledgments

The principal investigator wishes to thank J.G. Marvin for his general guidance in this research and Dr. T.J. Coakley for his guidance and insightful discussions throughout this work. The author is also grateful to Dr. C.C. Horstman for their helpful discussions on the 3-D SWBLI numerical simulations. This research was performed in the Modeling and Experimental Validation Branch at NASA Ames Research Center and supported by a grant from NASA to MCAT Institute (NCC 2-585).

References

1. Bardina, J., Coakley T., and Marvin J.: "Two-Equation Turbulence Modeling for 3-D Hypersonic Flows," *AIAA-92-5094*, Orlando, Florida, December 1992.
2. Coakley, T.J., and Huang, P.G., "Turbulence Modeling for High Speed Flows," *AIAA-92-0436*, Reno, Nevada, Jan. 1992.
3. Menter, F.: "Improved Two-Equation $k-\omega$ Turbulence Models for Aerodynamic, Flows," *NASA TM 103975*, October 1992.
4. Rodi, W.: "Experience with Two-Layer Models Combining the $k-\epsilon$ Model with a One-Equation Model near the Wall," *AIAA-91-0216*, Reno, Nevada, January 1991.
5. Settles, G.S., and Dodson, L.J..: "Hypersonic Shock/ Boundary Layer Interaction Database," *NASA CR 177577*, April 1991.
6. Kussoy, M.I., and Horstman, K.C.: "Documentation of Two- and Three- Dimensional Shock-Wave/ Turbulent Boundary Layer Interaction Flows at Mach 8.2," *NASA TM 103838*, May 1991.
7. Kussoy, M.I., and Horstman, K.C.: "Intersecting Shock- Wave/ Turbulent Boundary Layer Interaction at Mach 8.3," *NASA TM 103909*, February 1992.
8. Garrison, T.J., and Settles, G.S.: "Interaction Strength and Model geometry Effects on the Structure of Crossing - Shock Wave/ Turbulent Boundary Layer Interactions," *AIAA-93-0780*, Reno, Nevada, January 1993.
9. Bahrami, P.,: (private communication).
10. Kussoy, M.I., and Horstman, C.C.: (private communication).

Adiabatic Flat Plate

- $M_\infty = 5.$
- $Re_\theta = 10^4.$
- Turbulence models:
  - $k - \epsilon$ Launder-Sharma.
  - $k - \omega$ Wilcox.
  - $k - \omega$ baseline (includes algebraic length scale limit and rapid compression modifications).
  - $k - \omega$ with rotation modification.

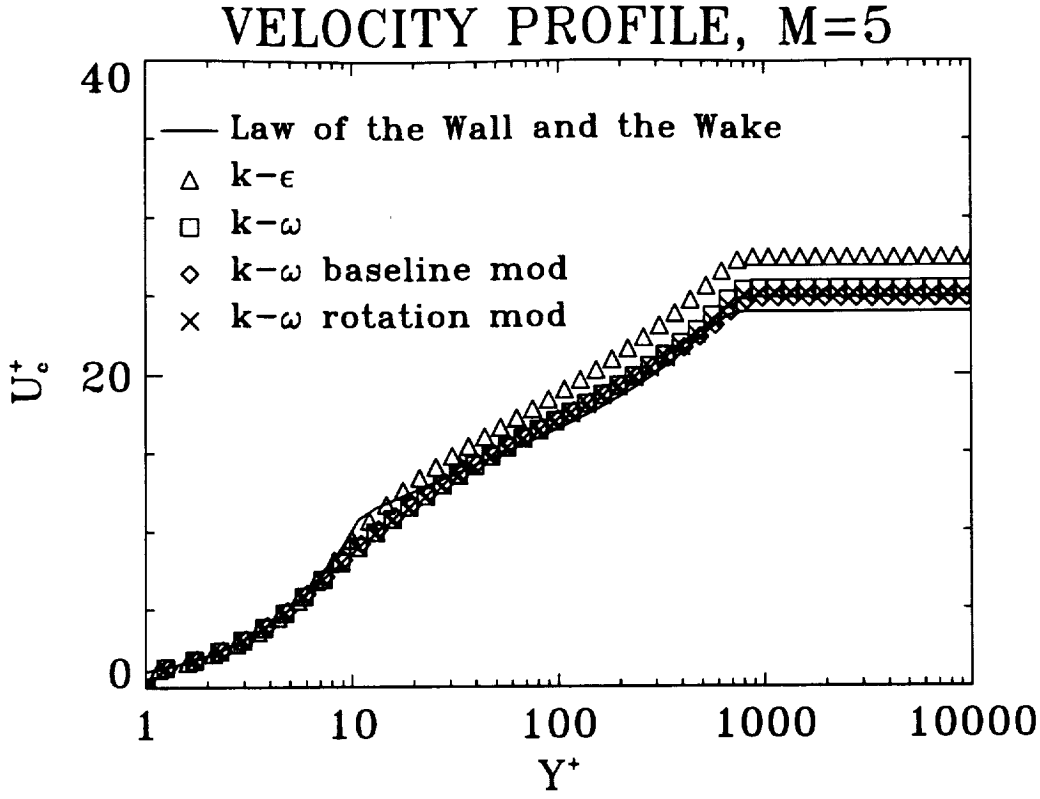
VELOCITY PROFILE, M=5
40
20
0
U_e^+
Law of the Wall and the Wake
k−ϵ
k−ω
k−ω baseline mod
k−ω rotation mod
1
10
100
1000
10000
Y^+

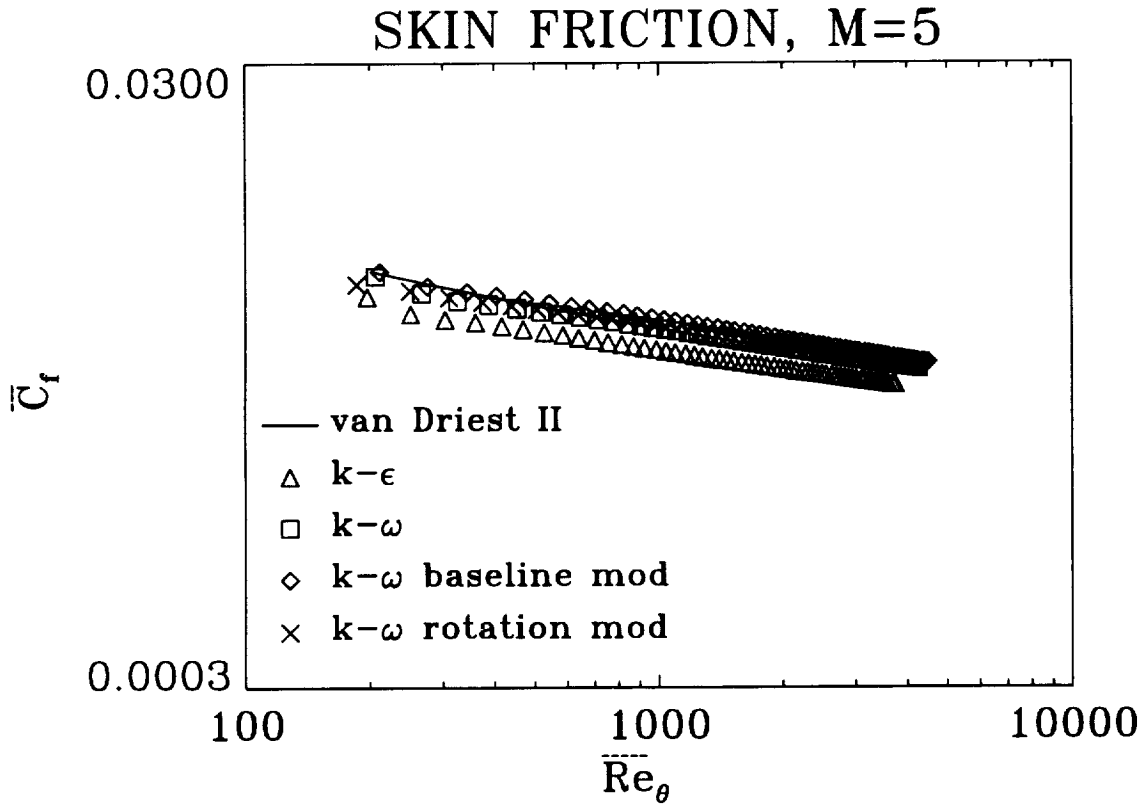
SKIN FRICTION, M=5
0.0300
0.0003
$\bar{C}_f$
van Driest II
k−ϵ
k−ω
k−ω baseline mod
k−ω rotation mod
100
1000
10000
$\overline{Re}_\theta$

Supersonic Compression Corner

- Settles' 24° compression corner, $M_\infty = 2.84$.
- Turbulence models:
  - $k-\omega$ Wilcox.
  - $k-\omega$ baseline (includes algebraic length scale limit and rapid compression modifications).
  - $k-\omega$ wlr-mod (includes baseline and rotation modifications).
  - $k-\omega$ l-mod (includes algebraic length scale limit modification).
  - $k-\omega$ r-mod (includes rapid compression modification).

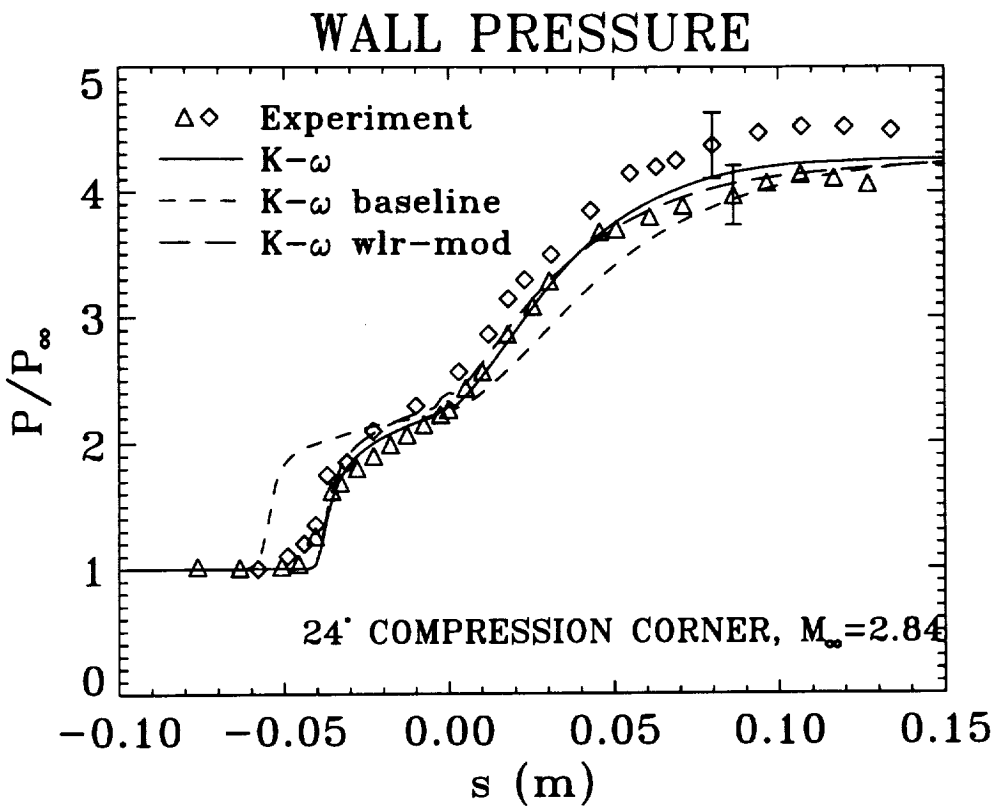
WALL PRESSURE
Experiment
K–ω
K–ω baseline
K–ω wlr–mod
24° COMPRESSION CORNER, M∞=2.84
P/P∞
s (m)
0
1
2
3
4
5
−0.10
−0.05
0.00
0.05
0.10
0.15

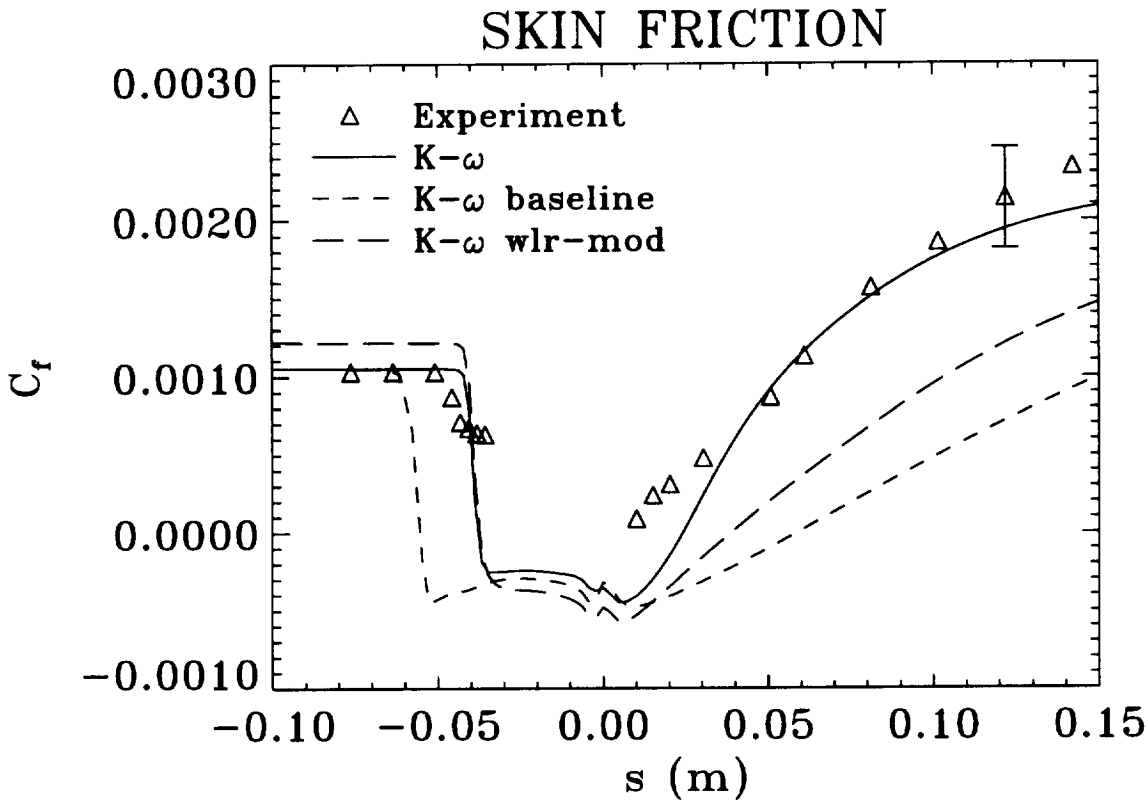
SKIN FRICTION
Experiment
K–ω
K–ω baseline
K–ω wlr–mod
Cf
s (m)
0.0030
0.0020
0.0010
0.0000
−0.0010
−0.10
−0.05
0.00
0.05
0.10
0.15

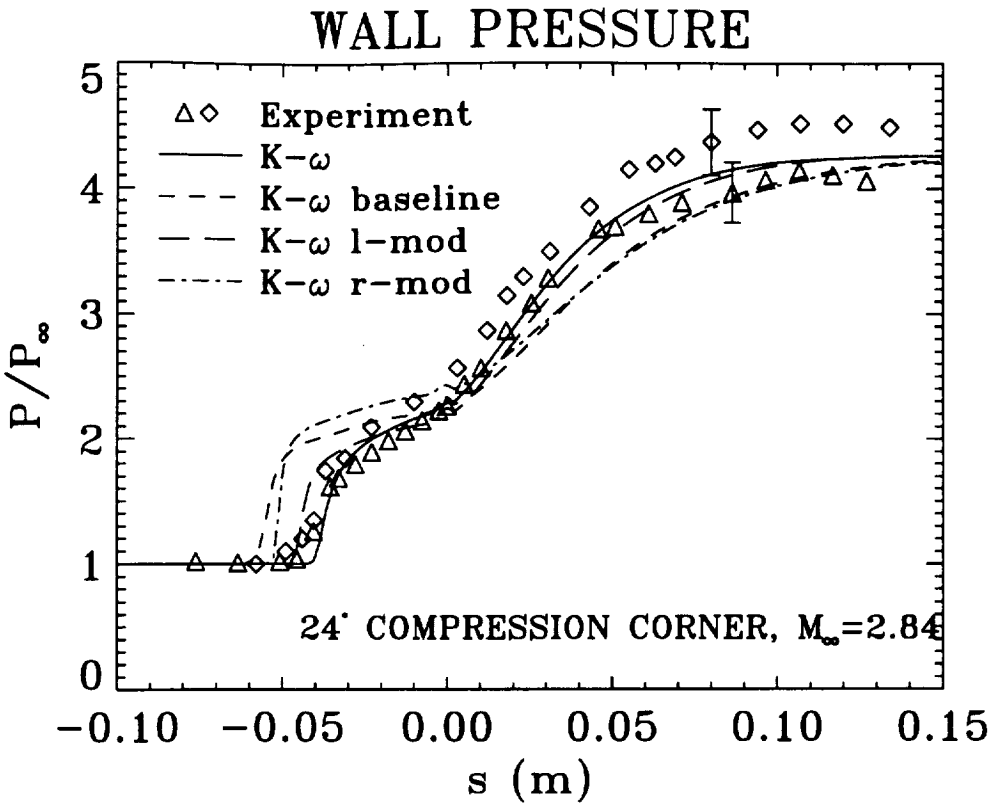
WALL PRESSURE
Experiment
K−ω
K−ω baseline
K−ω l−mod
K−ω r−mod
24° COMPRESSION CORNER, M∞=2.84
P/P∞
s (m)
0
1
2
3
4
5
−0.10
−0.05
0.00
0.05
0.10
0.15

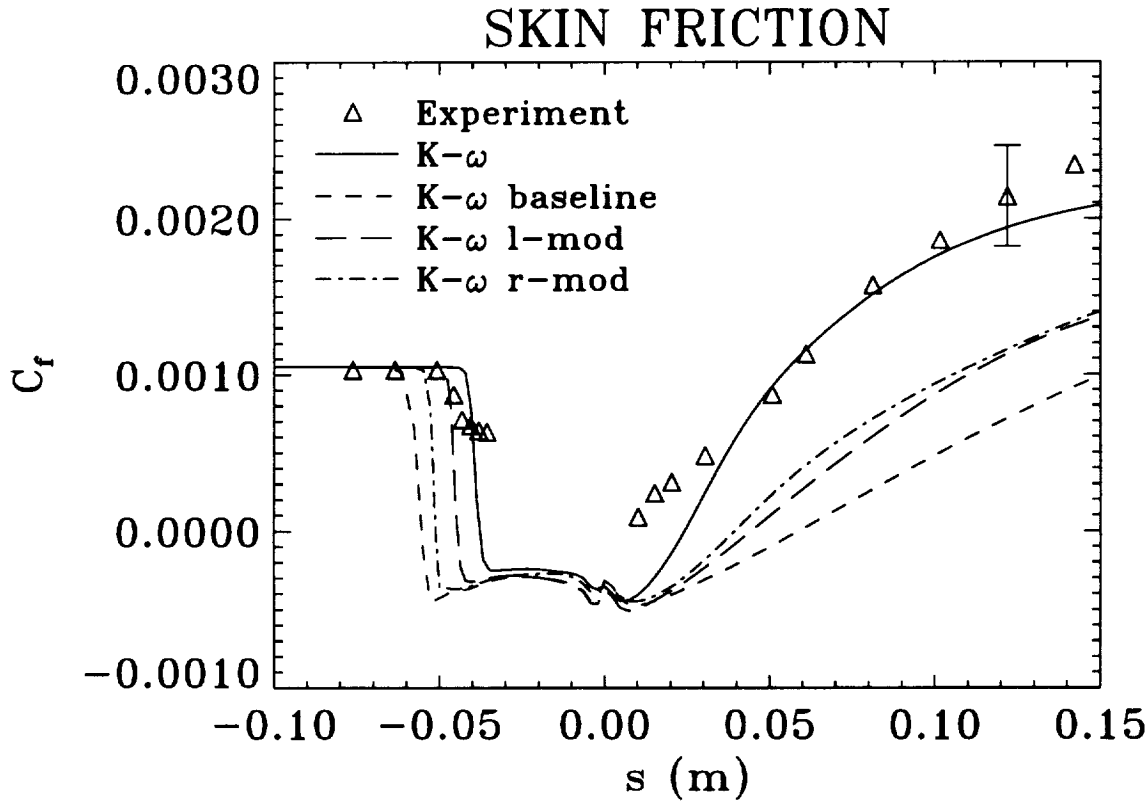
SKIN FRICTION
Experiment
K−ω
K−ω baseline
K−ω l−mod
K−ω r−mod
Cf
s (m)
0.0030
0.0020
0.0010
0.0000
−0.0010
−0.10
−0.05
0.00
0.05
0.10
0.15

APPENDIX A

AIAA-92-5064

Two-Equation Turbulence Modeling for 3-D Hypersonic Flows

J. Bardina,
MCAT Institute,
San Jose, CA
T. Coakley & J. Marvin,
NASA Ames Research Center,
Moffett Field, CA

AIAA FOURTH INTERNATIONAL AEROSPACE PLANES CONFERENCE
1 - 4 DECEMBER 1992/ORLANDO, FL

TWO-EQUATION TURBULENCE MODELING FOR 3-D HYPERSONIC FLOWS

J.E. Bardina*
MCAT Institute
San Jose, California

T.J. Coakley† and J.G. Marvin†
NASA Ames Research Center
Moffett Field, California

ABSTRACT

An investigation to verify, incorporate and develop two-equation turbulence models for three-dimensional high speed flows is presented. The current design effort of hypersonic vehicles has led to an intensive study of turbulence models for compressible hypersonic flows. This research complements an extensive review of experimental data and the current development of 2-D turbulence models. The review of experimental data on 2-D and 3-D flows includes complex hypersonic flows with pressure profiles, skin friction, wall heat transfer, and turbulence statistics data. In a parallel effort, turbulence models for high speed flows have been tested against flat plate boundary layers, and are being tested against the 2-D database. In the present paper, we present the results of 3-D Navier-Stokes numerical simulations with an improved $k-\omega$ two-equation turbulence model against experimental data and empirical correlations of an adiabatic flat plate boundary layer, a cold wall flat plate boundary layer, and a 3-D database flow, the interaction of an oblique shock wave and a thick turbulent boundary layer (SWBLI) with a free stream Mach number $M_\infty = 8.18$ and Reynolds number $Re_\infty = 5 \cdot 10^6$.

INTRODUCTION

The cost-effective engineering design of new vehicles encountering subsonic, transonic, supersonic, and hypersonic speeds requires an advanced and efficient computational fluid dynamics (CFD) technology for the accurate aerodynamic prediction of the complex 3-D flow fields. The CFD development as a design tool of complex vehicles with complex flow fields is based on advances in the understanding of the physics of the flows, experimental observations of turbulent flows, advances in numerical methods, and availability of faster numerical processors with large memory capacity. This method is needed to accurately predict the critical aerodynamic loads and wall heating rates in the design of hypersonic vehicles. The combination of an efficient three dimensional CFD shock capturing method with an accurate turbulence model is here required to account for the effects of the interaction of a planar shock wave which sweeps across the turbulent boundary layer. If the fin angle is large, the wall pressure rise and the boundary layer cause the formation of a strong crossflow separation vortex below the inviscid shock wave and inside the turbulent boundary layer. Part of the flow over the separation vortex reattaches behind the vortex impinging on the plate and leading to larger increments of wall pressure, skin friction, and heat transfer.

The interaction of shock waves with turbulent boundary layers causes considerable efficiency losses and represents a major design problem of vehicles flying at hypersonic speeds. This kind of interactions determines the performance of inlets for airbreathing propulsion at hypersonic speeds. Extensive experimental studies have been conducted for the 3-D sharp fin/ flat plate geometry[1-7]. Shock wave/ boundary layer interactions is the first specific topic of the hypersonic database collection and assessment effort of the critical review sponsored by the NASP program through NASA Ames Research Center[1]. This database collection has been generated to provide a common base for testing hypersonic turbulence models. This collection was based on a review of a survey of thousands of references which was narrowed to 105 distinct experimental studies. The experiments were subject to a database assessment and a few of them were reported in Category I[2] (accepted) or Category II[3,4] (limited acceptance). The data include wall pressure, skin friction, wall heat transfer, and flow field surveys at supersonic/ hypersonic free stream Mach numbers 3 through 6, with an inviscid pressure ratio across the planar shock varying from 1.35 to 5.1, respectively. At this time, the database is under further study in order to include new hypersonic experimental data.

Recently, an experimental study at Mach 8.18 was

*Consultant, NASA Ames Research Center, MS 229-1, Moffett Field, CA 94035.

†Member AIAA.

conducted by Kussoy and Horstman[6-8]. This study includes measurements of pressure profiles, skin friction, and surface heat transfer with 5°, 7.5°, 10°, 12.5°, and 15° fin angles. The experimental data also include flow field yaw angles and pitot pressures with 10° and 15° fin angles, corresponding to an inviscid pressure ratio of 5.4 and 9.7, respectively. Computational studies by Knight, Horstman, and Monson[8] include 3-D Reynolds averaged Navier-Stokes simulations with two $k-\epsilon$ turbulence models and a "conical" simulation with the Baldwin-Lomax mixing length turbulence model. Their 3-D Navier-Stokes simulation shows agreement with the experimental measurements of surface pressure, skin friction, flow direction, and wall heat transfer on the plate; it failed to predict the initial heat transfer peak and pressure valley observed below the inviscid shock wave; and the peaks of the heat transfer rate distributions are overpredicted by 36% and 48% in the 10° and 15° fin angle, respectively. The heat transfer rate on the fin section is overpredicted by a factor of 2 approximately, "due to the assumption of fully turbulent flow from the fin leading edge." The simulation with a laminar boundary layer on the fin overpredicts the heat transfer data inside the boundary layer thickness and agrees with the data outside of the boundary layer edge. Although the experimental boundary layer is laminar on the fin above the flat plate boundary layer, the simulations with turbulent and laminar flow on the fin show similar results of pressure, skin friction, and heat transfer on the flat plate. On the other hand, the "conical" simulations show poor agreement with experimental measurements. The wall pressure in the fin/ plate intersection zone is overpredicted by at least 25%, while the peak heat transfer rate is overpredicted by at least 200%. These differences were "attributed to the limitations of the Baldwin-Lomax turbulence model and/or the assumption of conical flow." The present simulations shown in this paper indicate that their differences are mostly due to their "conical" flow assumption.

Several experimental investigators[9-11] have been advancing the assumption of quasi-conical symmetry based on the empirical and numerical observations that the interaction vortex grows with distance following the direction of the inviscid oblique plane shock wave. This approximation is supported by the wall pressure data at lower Mach numbers in zones far from the fin leading edge and far from the intersection of the flat plate and the fin[11]. It is not supported by mean surface data of skin friction and heat transfer rate[5,12]. The main purpose of using conical coordinates in numerical simulations is to reduce the computer time needed to solve these flows and to increase the grid resolution. In general, the quasi-conical simulation[5] required about 1.2 hours of Cray-YMP with a 98x88 grid and about 3.6 hours of Cray-YMP with a 195x191 fine grid, while the 3-D Navier-Stokes simulations[8,13] with the hybrid explicit-implicit algorithm of MacCormack[14] required about 25 hours of Cray-YMP with a 64x40x60 grid.

Parallel to the experimental research effort, turbulence models for high speed flows are currently being developed and tested for the design of hypersonic vehicles. These models include different versions of the $k-\epsilon$ and $k-\omega$ two equation turbulence models[15]. The numerical results show good agreement within 10% of skin friction measurements and empirical correlations in adiabatic and cooled-wall flat plate boundary layers ($0.2 \leq T_w/T_{aw} \leq 1.0$ and $M_\infty \leq 10$). Their heat transfer predictions show a Reynolds analogy factor of 1.17 to 1.19. This kind of agreement is also observed when the proposed modeling compressibility corrections for complex flows are incorporated into the models. Several corrections have been proposed to reduce the overprediction of mean heat transfer rates in reattachment zones of separating boundary layers, to increase the size of flow separation and the corresponding surface pressure distributions, and to reduce the spreading rate of turbulent shear layers. to improve the prediction of flow separation. These turbulence model corrections showed significant improvements in the wall pressure and mean heat transfer rate predictions of 2-D shock wave/ boundary layer interactions[16]. Numerical simulations are beginning to provide significant results in engineering design; in particular, efficient computational fluid dynamics (CFD) methods are beginning to serve as major complement to wind tunnel experimental research due to the latest advances in CFD and available computer power.

The objectives of this paper are to evaluate a baseline $k-\omega$ model in a strong shock wave/ boundary layer interaction, to examine the capability of the simulation to represent the complex 3-D structure of the flowfield, and to demonstrate the capability of a new efficient 3-D computational Navier-Stokes method with a two-equation turbulence model.

3-D NUMERICAL METHOD

The numerical method[17] is based on a 3-D implicit upwind flux-difference split finite difference algorithm of the mean compressible Navier-Stokes equations using mass-averaged variables. The conservation laws of mass, momentum, and energy for the 3-D Navier-Stokes equations are expressed in generalized curvilinear coordinates and in compressed vector notation as

$$(JU)_{,t} + \overline{J\xi_{i,j}}\, F_{j,\bar{i}} = 0 \qquad (1)$$

where repeated sub-indices in any term imply summation over the index range, sub-index t following a comma implies partial differentiation with respect to time, sub-index j following a comma implies partial

differentiation with respect to the spatial Cartesian coordinate direction x_j, sub-index $\tilde{i}$ following a comma implies partial differentiation with respect to the spatial curvilinear coordinate direction ξ_i, and the overbar denotes spatial averaging. The vector U represents the conservative dependent variables,

$$U = (\rho, \rho u_1, \rho u_2, \rho u_3, e) \qquad (2)$$

F_j are the flux vectors in the respective Cartesian coordinates direction x_j, and J is the Jacobian of the coordinate transformation. The metric coefficients are evaluated at the interface between the grid points of the spatial difference.

All flux differences are treated implicitly in order to increase stability and to be able to use large increments of time or CFL numbers. The numerical scheme for the viscous fluxes is second-order central difference, while the numerical scheme for the inviscid fluxes is a higher-order TVD upwind flux-difference splitting. Different tests and experiments in subsonic, transonic, and supersonic flows have shown that the conservation properties are maintained once convergence is achieved with a second- or higher-order scheme[18,19].

The differentiation of the inviscid fluxes is similar to Roe's flux difference splitting method, however it is based on simple arithmetic averaging of primitive variables. In order to preserve the conservative property of the fluxes, each flux difference term $F_{j,\tilde{i}}$ of the conservation law equations is defined as

$$\delta F = F_{\tilde{i}+1} - F_{\tilde{i}} = A\,\delta U = S\Lambda S^{-1}\,\delta U \qquad (3)$$

where the subindex j is omitted in equation 3 for simplicity. Λ is a diagonal matrix whose coefficients are the eigenvalues of the matrix A, and S is the column-eigenvector matrix of A. The inviscid first-order flux differences terms are split according to the sign of the eigenvalues and unconditionally stable Euler implicit methods are constructed by backward upwind differencing flux differences with positive eigenvalues and forward differencing flux differences with negative eigenvalues.

Higher-order spatial TVD flux differences in the right-hand-side of the inviscid terms of the conservation law equations are defined by using the "*minmod*" limiter of Osher and Chakravarthy[20] applied on the complete split flux difference instead of the characteristic variable difference. It has the capability to represent various higher-order differences: first-order upwind, second-order upwind, third-order upwind biased, second-order Fromm scheme, and other combinations of upwind and central differences.

The solution procedure is based on an implicit "method of planes" symmetric Gauss-Seidell relaxation scheme. The data is conveniently stored on successive planes along the streamwise coordinate, and the system of equations is solved in each successive plane along the forward direction, first, and along the backward direction, afterwards In each plane, the solution is obtained by using a two level pseudo time dependent relaxation procedure based on a diagonally dominant approximate factorization DDADI. The space marching alternating directional sweeps in the streamwise direction are von Neumann unconditionally stable for zones of subsonic and streamwise separated and reversed flows as well as supersonic flow. The space marching method results in improved propagation of nonlinear effects to accelerate convergence to steady state, much as do the more restrictive PNS techniques[18,19].

The diagonal dominant approximate factorization of the left-hand-side of the conservation law equations including the implicit viscous terms leads to the following block tridiagonal equation sequence for the ξ_1 plane relaxation method

$$(-A^+_{\xi_2},\, D,\, A^-_{\xi_2})\,\delta U^* = -RHS^{n,n+1} \qquad (4a)$$

$$(-A^+_{\xi_3},\, D,\, A^-_{\xi_3})\,\delta U \;= -D\,\delta U^* \qquad (4b)$$

The diagonally dominant matrix D involves the first-order split Jacobian matrices and the Jacobian matrices of the viscous terms of each coordinate direction and the solution is updated from time step n to time step $n+1$. Observe that the RHS of equation 4a has an exponent $n, n+1$ because some terms in the streamwise direction are already updated at time step $n+1$ due to the plane relaxation procedure.

A Newton-Raphson acceleration procedure is obtained by solving each plane twice or more times in each relaxation sequence. This procedure produces significant improvement in the propagation of nonlinear effects due to the nonlinearity of the Jacobian matrix.

BOUNDARY CONDITIONS

Mathematically well posed implicit boundary conditions are imposed in every grid boundary point. These conditions are mathematically well posed and based on the sign of the eigenvalue of the corresponding component of the flux-difference split vector. The physical boundary approximations imposed on the calculations are frozen inflow, no slip velocity and adiabatic or cold temperature on the wall surface, symmetry plane, and flow through in free boundaries. The inflow profiles are defined by the free stream values on the flat plate calculations, and on the flat plate profiles with matching δ^* experimental values on the fin/flat plate calculations. At the flow through and outflow boundary planes, if the flow is subsonic inflow then no change in entropy, enthalpy and tangential velocity are imposed, and if the flow is subsonic outflow

then no pressure variation is imposed in the differencing toward the boundary. Free stream static pressure is effectively maintained, and outflow boundary data is properly extrapolated by the algorithm. The symmetry plane condition is applied to the grid points on the plane upstream of the fin leading edge.

TURBULENCE MODELS

Two kind of turbulence models have been used in these simulations. The first kind of model is the $k-\omega$ two-equation turbulent eddy viscosity model[15]. The eddy viscosity is defined as

$$\mu_\tau = c_\mu \rho k/\omega \tag{5}$$

where k and ω are the additional field variables. Observe that ω is defined as ϵ/k whereas the traditional formulation is $\epsilon/c_\mu k$. The $k-\omega$ field equations are written as

$$(J\rho k)_{,t} + \overline{J\xi_{i,j}}\,(\rho k u_j)_{\bar{i}} = J(c_{k1}P - c_{k2}\rho\omega k) - (\overline{J\xi_{i,m}}(\mu + \mu_\tau/\sigma_k)\bar{\xi}_{j,m}k_{,\bar{j}})_{,\bar{i}} \tag{6}$$

$$(J\rho\omega)_{,t} + \overline{J\xi_{i,j}}\,(\rho\omega u_j)_{\bar{i}} = J(c_{\omega 1}P\omega/k - c_{\omega 2}\rho\omega^2) - (\overline{J\xi_{i,m}}(\mu + \mu_\tau/\sigma_\omega)\bar{\xi}_{j,m}\omega_{,\bar{j}})_{,\bar{i}} \tag{7}$$

where P the production of turbulent kinetic energy is

$$P = \mu_\tau((u_{i,j} + u_{j,i})u_{i,j} - u_{i,i}u_{j,j}2/3) - \rho k u_{i,i}2/3 \tag{8}$$

and the model constant or parameters are

$$\begin{array}{llll} c_{k1} = 1.0 & c_{\omega 1} = 0.555 & \sigma_k = 2.0 & c_\mu = 0.09 \\ c_{k2} = 1.0 & c_{\omega 2} = 0.833 & \sigma_\omega = 2.0 & \end{array} \tag{9}$$

This model does not need explicit damping terms in the model parameters due to the behavior of ω in the wall layer, although Wilcox[21] has proposed a low turbulent Reynolds number dependence of the model parameters (c_μ, c_{k2}, and $c_{\omega 1}$) in order to describe transition in simple 2-D flows. The boundary conditions at the wall are $k = 0$ and $\omega = 6\mu/(c_{\omega 2}\rho y_1^2)$ where y_1 is the wall distance from the first grid point off the wall. No difference is found if ω is redefined after each iteration by the minimum value between ω itself and $6\mu/(c_{\omega 2}\rho y^2)$ within the laminar sublayer, however, there is an improvement in convergence speed.

The modeling correction for reduction in the prediction of heat transfer rate in the reattachment zone is based on an algebraic upper limit of the turbulent length scale near the wall[15]. This limit is defined by the Prandtl length scale, κy, and it is used to redefine the specific dissipation rate $\omega = \sqrt{k}/l$ by the following relationship,

$$l = min(c_\mu^{-3/4}\kappa y, \sqrt{k}/\omega) \text{ and } \kappa = 0.41 \tag{10}$$

This modification is mainly significant near reattachment and has little effect in other zones[15,16,22]. The modeling correction to increase the separation bubble size is based on the assumption that the product ρl remains constant under rapid compression and it adds a term proportional to the dilatational term, $-2\rho k u_{i,i}/3$, $-J2/3(2 - c_{\omega_1})\rho\omega u_{i,i}$ to the right-hand-side of the ω eq. 7. In other words, the net contribution of the dilatational term, including the last production term of Eq. 8, is increased from $-J2/3c_{\omega_1}\rho\omega u_{i,i}$ to $-J4/3\rho\omega u_{i,i}$. The $k-\omega$ model including the length scale and the rapid compression modifications is called the baseline $k-\omega$ model.

The second kind of model is an algebraic turbulent eddy viscosity model based on the Baldwin and Lomax[23] formulation. This model is a two-layer mixing length formulation for the eddy viscosity similar to the mixing length model of Cebeci[18]. The inner layer uses the Prandtl- Van Driest formula with a lower bound value of 1/14 of the maximum viscosity value in free shear zones, while the outer layer uses a function of the maximum value of the mean vorticity and total velocity difference.

DESCRIPTION OF THE SIMULATIONS

The computational grids have been generated using simple algebraic cubic interpolation and clustering to the wall boundaries. The number of grid points in these simulations are 3x61x61 for the Mach 5 flat plate flow (see Fig. 1a), 91x61x3 for the Mach 8.18 flat plate flow (see Fig. 2a), and 61x41x61 for the Mach 8.18 3-D oblique shock wave - turbulent boundary layer interaction flow (see Fig. 3). The Mach 5 flat plate grid has 3 parallel planes to the mean flow, and the solution procedure applied was the diagonally dominant approximate factorization in the midplane. The value of y^+ for the first grid point off the wall varied from 0.2 to 0.35, and about 45 grid points were located inside the boundary layer. The Mach 8.18 flat plate grid has 91 planes along the mean flow, and the solution procedure was the plane relaxation with four inner Newton-Raphson iterations. The value of y^+ for the first grid point off the wall was 0.02, and about 40 grid points were located inside the boundary layer. This grid was clustered to the wall and to the leading edge in order to provide the initial profiles for the shock wave - boundary layer interaction (SWBLI). The 61x41x61 grid is similar in topology to the 64x40x64 grid used by Knight et al[8] in a previous 3-D SWBLI computation. Each longitudinal grid line along the flat plate has 61 grid points from the inflow through the outflow plane; each grid line normal to the flat plate has 41 grid points from the plate through the outer-flow plane; and each grid line normal to the mean flow direction and the flat plate has 61 grid points from the fin through the free flow lateral plane. A coarser

31x21x31 grid which uses every other grid point of the finer 61x41x61 grid was used to achieve faster convergence time, to examine different model corrections, and to examine grid effects in this simulation. The solutions of the coarse grid were used to provide the initial flowfield of the fine grid. Figure 3 shows a 3-D view of the grid points located on the flat plate and the fin surface. The minimum grid point spacing normal to the walls has been fixed to $4 \cdot 10^{-6} m$; in wall coordinates, the grid point spacing at the inflow section of the plate is $y^+ = 0.08$. the solution procedure used the plane relaxation in the streamwise direction and the diagonally dominant approximate factorization along the curvilinear coordinates on the plane.

The 3-D Navier-Stokes simulations of the SWBLI with the coarser grid required between 30 to 50 minutes, while the simulations with the finer grid required between 3 to 6 hours of CRAY-YMP cpu time. The adiabatic and cooled-wall flat plate simulations required only a few minutes of cpu time.

All the simulations assume perfect air with constant ratio of specific heat $\gamma = 1.4$, molecular Prandtl number 0.73, and turbulent Prandtl number 0.9. The laminar viscosity is specified by Sutherland's law[24].

ADIABATIC FLAT PLATE FLOW, $M_\infty = 5$

The main objectives of the adiabatic flat plate calculations were to verify the 3-D numerical simulations and the turbulence models. Following the detailed comparison of Coakley and Huang[15] in the development and testing of two-equation models in 2-D flows, a comparison with empirical correlations of experimental data and other numerical simulation is presented. The mean flow conditions are $M_\infty = 5$, $T_w/T_{aw} = 1$, and $Re_\infty = 2.2 \cdot 10^7$ per meter. This Reynolds number avoid low Reynolds number effects[4]. Figure 1b shows the comparison of the van Driest II empirical correlation, the skin friction results using the van Driest compressible transformation[25] shows excellent agreement with the Karman-Schoenherr correlation curve[26] as a function of the momentum thickness Reynolds number. Figures 1c and 1d show the comparisons of the velocity profile with the compressible law of the wall[25] in wall coordinates, and the 2-D prediction of Coakley et al[15], respectively. The results show very good agreement in the prediction of the law of the wall and velocity profile obtained with a different 2-D code[15]. As it is expected, there is little difference between the results obtained with the $k-\omega$ model with and without the proposed modeling corrections described in the turbulence models section.

COLD FLAT PLATE FLOW, $M_\infty = 8.18$

The cold flat plate flow calculations were done to simulate the experimental results of Kussoy et al[4], in order to provide the initial profiles of the SWBLI simulations described below, and to verify the 3-D numerical simulations. The mean flow conditions are $M_\infty = 8.18$, $T_w/T_{t\infty} = 0.27$, $T_w/T_{aw} = 0.3$, and $Re_\infty = 5 \cdot 10^6$ per meter. Following the detailed comparison of Coakley and Huang[4] in the development and testing of two-equation models a comparison with empirical correlations of experimental data and other numerical simulation is presented at Figure 2b shows the comparison of the van Driest II empirical correlation, the skin friction results using the van Driest compressible transformation[25] with the Karman-Schoenherr correlation curve[26]. The results obtained with the $k-\omega$ with and without the length-scale and the rapid compression modifications are about 10% higher than those results predicted with the empirical correlation, while the results obtained with the Baldwin-Lomax algebraic model tend to agree with the empirical correlation at higher momentum thickness Reynolds numbers. The differences in the results may be smaller at higher Reynolds numbers. In order to test the predictions at higher Reynolds numbers, the flat plate was extended from the original length of 2.2 meters upto a length of 3 meters in the numerical simulations, However, the transformed momentum thickness Reynolds number was still less than 3000. Figure 2c shows the velocity profile comparison with the compressible law of the wall[25] in wall coordinates. These predictions are also similar to the 2-D prediction of Coakley et al[15] and they underpredict the law of the wall. Figure 2d show the full cold wall velocity profiles obtained with the different models. The main differences in the profiles are observed in the wake region of the velocity distributions. Figure 2e show the typical growth of the Mach contour lines inside the turbulent boundary layer obtained with the modified $k-\omega$ model, the growth rate of each contour line is almost linear and uniform. Figure 2f shows the pressure contour levels normalized with the free stream pressure and the main feature is the pressure rise caused by the lip shock.

OBLIQUE SHOCK WAVE - TURBULENT BOUNDARY LAYER INTERACTION

The experiment was conducted with free stream Mach number $M_\infty = 8.18$, temperature $T_\infty = 81K$, and pressure $p_\infty = 430 N/m^2$. The flat plate dimensions were 2.2 m length and 0.76 m width, while the fin dimensions were 0.3 m length and 0.2 m height. The fin was mounted 1.76 m downstream of the flat plate leading edge. Both the fin and flat plate were cooled with a temperature of $300°K$ which is equivalent to $T_w = 0.27 T_{t\infty} \equiv 0.3 T_{aw}$. The free stream Mach number is 8.18 and the free stream Reynolds number is $5 \cdot 10^6$ per meter.

The inflow profiles for the 3-D SWBLI simulations were obtained from the flat plate profiles that matched the experimental value of the compressible displacement thickness, $\delta^* = 0.0159m$. The experiment was done on a flat plate with $-2°$ angle of attack in order to attain a uniform 2-D inflow before the fin interaction zone. 3-D Navier-Stokes simulations of the flat plate flow were run with and without angle of attack. As it should be expected, differences are mainly obtained in the magnitude of the primitive variables inside the shock layer. Since most of the experimental results are nondimensionalyzed with shock layer values, the inflow boundary layer profiles were generated by running a Navier-Stokes simulation of the flat plate flow from the leading edge with no angle of attack. The following Figures 4 through 6 show the velocity, temperature, and density profiles, respectively, of the 3-D flow obtained with the $k-\omega$ turbulence model including the modeling corrections. The numerical results are shown in solid lines while the experimental results are shown with diamond symbols. There are small differences in the boundary layer profiles caused by the difference in the angle of attack of the flat plate.

Results for $\alpha = 10°$ and $15°$

The 3-D Navier-Stokes SWBLI simulations were done with a $10°$ and a $15°$ fin angle. Both geometries were simulated with both the coarser 31x21x31 and the finer 61x41x61 grids. In the experiment, the boundary layer on the flat plate was thick and turbulent, while the boundary layer on the fin surface was laminar above the flat plate boundary layer edge. The estimated transition location of the fin boundary layer was downstream of the test section of the experimental data[8]. The fin surface was simulated as a laminar boundary layer and also as a turbulent boundary layer, the results show only significant differences in the prediction of the heat transfer rate on the fin surface; this observation is also supported by previous simulations[8]. Results obtained with four different turbulence models are reported in this paper: the baseline $k-\omega$, the standard $k-\omega$, the transitional $k-\omega$ model[21], and the two-layer algebraic Baldwin-Lomax turbulence models. Both geometries were simulated with the baseline $k-\omega$ and the standard $k-\omega$ models. In addition, the flat plate with the $10°$ fin angle was also simulated with the Baldwin-Lomax turbulence model and the transitional $k-\omega$ model[21]. The transitional $k-\omega$ model was used to test its predictive capabilities of the heat transfer rate data on the fin surface.

In the following figures, the symbols show the experimental data, the vertical lines on the symbols show the experimental uncertainty of the data, and the different lines show the numerical results. x is the distance on the flat plate from the fin leading edge along the main freestream flow, $s = x/cos\alpha$ is the distance along the fin/plate junction from the fin leading edge, the abscissa $z - xtan\alpha$ represents the distance from the fin along the crossed section of the flat plate, and y represents the vertical distance along the surface of the fin. Figures 5 and 6 show the comparison of the results obtained for the $10°$ and the $15°$ fin angle, respectively.

• The Plate Surface Pressure

Figures 5a and 6a show the comparison of the surface pressure profile against the experimental data on the flat plate surface at $x = 0.1819$ m as a function of distance from the fin, for the $10°$ and $15°$ fin angles, respectively. The ordinate P/P_∞ shows the nondimensional pressure values which are nondimensionalized with the freestream pressure. All the pressure profiles show the rise of the pressure in the boundary of the separation zone of the crossflow vortex, a plateau in the separation zone, and a peak pressure in the reattachment zone behind the vortex and very near the fin. The agreement between the predictions of the baseline $k-\omega$, the standard $k-\omega$, and the Baldwin-Lomax models and the experimental data is quite good, especially in the $10°$ fin angle case within the 10% experimental uncertainty of the data. There is only an underprediction of the peak reattachment pressure in the $15°$ fin angle case which it may be caused by lack of grid resolution and/or turbulence modeling. Although, some improvements in the agreement with the experimental data were obtained with the 61x41x61 simulations, in particular, the low pressure values shown between the pressure plateau and reattachment peak. The results of the two-equation models are closer to the peak pressure data. The results with the baseline model are only slightly closer to the experimental data than those shown by the standard $k-\omega$ turbulence model. Furthermore, the results with the finer grid follow the peaks and valley of the pressure profile more closely, which may indicate that grid resolution may give an even better agreement. The pressure profiles on the flat plate are similar to the predictions of Knight et al[4] using a $k-\epsilon$ model; however, their "conical" solutions with the Baldwin-Lomax model are quite inferior and overestimate the peak pressure by 26% and 53% in the $10°$ and $15°$ fin angle, respectively. These differences should be attributed to their assumption of "conical" flow.

• The Fin Surface Pressure

Figures 5b and 6b show the comparison of the surface pressure profile against the experimental data obtained at $s = 0.1834$ m on the fin as a function of the vertical distance y from the flat plate along the fin surface, for the $10°$ and the $15°$ fin angle, respectively. The ordinate P/P_∞ shows the nondimensional pressure values which are nondimensionalized with the freestream pressure. All the numerical results obtained with the different turbulence models and grids show excellent agreement with the experimental data, in particular the baseline $k-\omega$ model with the finer grid. The pressure profiles show a peak in the fin/plate junction due to the reattachment jet stream, a decrease inside the turbulent boundary layer which may be a secondary effect of the jet stream behind the main crossflow vortex, and a rise upto a high pressure plateau due to the pressure increase caused by the oblique shock wave. The pressure profile predictions on the fin surface are a little better than those

presented by Knight et al[4] using a $k-\epsilon$ model, and much better than their "conical" solutions with the Baldwin-Lomax model which are quite inferior.

• The Plate Skin Friction

Figures 5c and 6c show the comparison of the surface skin friction profile against the experimental data on the flat plate at $x = 0.155$ m as a function of distance from the fin, for the 10° and the 15° fin angle, respectively. All the 3-D numerical simulations show good agreement with the experimental data. The peak skin friction in the reattachment zone is predicted within the uncertainty of the data. The predictions are similar to those presented by Knight et al[4] using a $k-\epsilon$ model, and much better than their "conical" solutions with the Baldwin-Lomax model which overestimate the peak value by 225% and 129% in the 10° and 15° fin angle cases, respectively. All the numerical predictions show a decrease in the skin friction very near the fin/plate corner zone. This behavior which is not evident from the experimental data is caused by a very small zone of cooled dead flow in the 90° corner walls. The predictions do not show any evidence of a second smaller local peak as indicated by the few available data. Further improvements in turbulence modeling is required to represent these effects of the vortical structure. The predictions of the baseline and the standard $k-\omega$ model are very similar.

• The Plate Heat Transfer Rate

Figures 5d and 6d show the comparison of the surface heat transfer rate profile against the experimental data on the flat plate at $x = 0.1645$ m as a function of distance from the fin, for the 10° and the 15° fin angle, respectively. The ordinate Q/Q_∞ shows the nondimensional heat transfer rate values which are nondimensionalized with the freestream inflow value upstream of the shock interaction. The experimental profiles show a rise along the separation boundary of the crossflow vortex, a plateau in the separation zone, and a peak value in the reattachment zone behind the crossflow vortex and near the fin. For the 15° fin angle, the experimental profile shows a decrease of the heat transfer rate between the plateau and the reattachment peak. The agreement between the predictions of the baseline $k-\omega$, the standard $k-\omega$, and the Baldwin-Lomax models and the experimental data is quite good. Although the two-equation models tend to underpredict the heat transfer rate under the separation zone, while the Baldwin-Lomax prediction is within the experimental uncertainty in the 10° fin angle case. The results of the simulations with the baseline and the standard $k-\omega$ models show reasonable agreement with the data in the 15° fin angle case. There is an underprediction of the peak heat transfer rate in the separation zone, and the decrease of the heat transfer rate between the plateau and the reattachment peak is not predicted. The peak heat transfer rate is predicted within the 10% experimental uncertainty in the 10° fin angle case, and slightly overpredicted by 14% (4% above the uncertainty of the data) in the 15° fin angle case. The predictions are also similar to those presented by Knight et al[4] using a $k-\epsilon$ model, however, their overpredictions of the peak heat transfer rate were much higher, 36% and 48%, respectively. Their "conical" solutions with the Baldwin-Lomax model are also quite inferior.

• The Fin Heat Transfer Rate

Figures 5e and 6e show the comparison of the surface heat transfer rate profile against the experimental data on the fin surface at $s = 0.167$ and $s = 0.1962$ m as a function of distance from the flat plate, for the 10° and the 15° fin angle, respectively. All the results with the two-equation models assuming fully turbulent flow from the fin leading edge overpredict the heat transfer rate by almost 175% in the laminar boundary layer. Close agreement is obtained when laminar flow is assumed on the fin wall. The transition $k-\omega$ model[21] overpredicts the heat transfer rate by almost 85%. The heat transfer rate on the fin surface near the corner inside the plate boundary layer is not well predicted. Further studies on transition and 3-D combination of laminar and turbulent boundary layers is needed. A simulation assuming turbulent boundary layer inside the plate boundary layer and transition modeling above the plate boundary layer edge did not improve the results.

• Pitot Pressure Profiles

Figures 5f and 6f show the comparison of the pitot pressure profiles against the experimental data as a function of distance from the flat plate. For the 10° fin angle, the data is at $x = 0.1723$ m and $z = 0.064$, 0.0127, 0.0191, 0.0254, 0.0381, and 0.0508 m. The results obtained with the standard $k-\omega$ model show close agreement with the experimental data. Small differences are observed near the intersection of the boundary layer edge and the oblique shock wave. For the 15° fin angle, the data is at $x = 0.1744$ m and $z = 0.0191$, 0.0254, 0.0381, 0.0508, 0.0635, and 0.0762 m. The results obtained with the baseline $k-\omega$ model show close agreement with the experimental data, except near the intersection of the boundary layer edge and the oblique shock wave.

• Pitot Pressure Contours

Figures 5g and 6g show the pitot pressure contours in the crossed section corresponding to the previous Figures 5f and 6f, respectively. The contour lines show the strong oblique shock and the wave structure of the of the main crossflow vortex. A comparison of the pitot pressure contours against the experimental data is shown in Figures 5h and 6h, respectively. The agreement is very good for the 10° fin angle case, although some differences are observed near the intersection of the turbulent boundary layer edge and the oblique shock wave. Similar results are observed for the 15° fin angle case, except for slightly larger differences in the crossflow vortex.

CONCLUDING REMARKS

A 3-D Navier-Stokes numerical simulation of the 3-D shock wave/ boundary layer interaction with a 10° and a 15° fin angle has been conducted. Comparisons between the results obtained with the baseline $k-\omega$, the standard $k-\omega$, and the Baldwin-Lomax algebraic model agree in general with the experimen-

tal data. The simulations with the baseline $k-\omega$ turbulence model provides excellent agreement with the adiabatic flat plate data, good agreement with the cooled flat plate data, and fairly good agreement with the complex shock wave/ boundary layer interaction data. The flow structures are fairly well capture, in particular, the external planar oblique shock and the shock-wave/ boundary layer interaction zone are free of oscillations. There is a need to improve the models in order to avoid the underprediction of heat transfer rate in the crossflow separation zone. The model of "conical" approximation of the flow is not supported by the present simulations. Finally, the present numerical simulations are very efficient and require less cpu time than previous simulations with other algorithms, which is an important requirement to test different turbulence models in complex flows.

ACKNOWLEDGEMENTS

This work is sponsored by NASA Ames Research Center under Grant NCC 2-15. The authors wish to acknowledge helpful discussions on turbulence modeling with P.G. Huang and shock wave/ turbulent boundary layer interactions with C.C. Horstman.

REFERENCES

1. Settles, G.S., and Dodson, L.J.: "Hypersonic Shock/ Boundary-Layer Interaction Database," *NASA CR 17757,* April 1991.
2. Law, C.H.: "3-D Shock Wave- Turbulent Boundary Layer Interactions at Mach 6," *ARL TR 75-0191,* 1974.
3. Kim, K.S., Lee, Y., Alvi, F.S., Settles, G.S., and Horstman, C.C.: "Laser Skin Friction Measurements and CFD Comparison of Weak-to-Strong Swept Shock/ Boundary Layer Interactions," *AIAA-90-0378,* January 1990.
4. Knight, D.D., Horstman, C.C., Bogdonoff, S.M., and Shapey, B.L.: "The Flowfield Structure of the 3-D Shock Wave - Boundary Layer Intercation Generated by a 20° Sharp Fin at Mach 3," *AIAA-86-0343,* 1986.
5. Rodi, P.E., Dolling, D.S., and Knight, D.D.: "An Experimental/ Computational Study of Heat Transfer in Sharp Fin Induced Turbulent Interactions at Mach 5," *AIAA-91-1764,* June 1991.
6. Kussoy, M.I., and Horstman, K.C.: "Documentation of Two- and Three- Dimensional Shock-Wave/ Turbulent Boundary Layer Interaction Flows at Mach 8.2," *NASA TM 103838,* May 1991.
7. Kussoy, M.I., Kim,K.S., and Horstman, K.C.: "An Experimental Study of a Three- Dimensional Shock-Wave/ Turbulent Boundary Layer Interaction at a Hypersonic Mach Number," *AIAA-91-1761,* June 1991.
8. Knight, D.D., Horstman, C.C., and Monson, D.J.: "The Hypersonic Shock Wave- Turbulent Boundary Layer Interaction Generated by a Sharp Fin at Mach 8.2," *AIAA-92-0747,* January 1992.
9. Settles, G.S., and Lu, F.K.: "Conical Similarity of Shock Wave/ Boundary Layer Interactions Generated by Swept and Unswept Fins," *AIAA J.,* Vol. 23, 1985, pp. 1021-1027.
10. Alvi, F.S., and Settles, G.S.: "A Physical Model of the Swept Shock/ Boundary-Layer Interaction Flowfield," *AIAA-91-1768, June 1991.*
11. Settles, G.S., and Dolling, D.S.: "Swept Shock/ Boundary Layer Interactions - Tutorial and Update," *AIAA-90-0375,* January 1990.
12. Knight, D.D., and Badekas, D.: "On the Quasi-Conical Flowfield Structure of the Swept Shock Wave- Turbulent Boundary Layer Interaction," *AIAA-91-1759,* June 1991.
13. Lee, Y., Settles, G.S., and Horstman, C.C.: "Heat Transfer Measurements and CFD Comparison of Swept Shock Wave/ Boundary Layer Interactions," *AIAA-92-3665,* July 1992.
14. MacCormack, R.: "A Numerical Method for Solving the Equations of Compressible Viscous Flow," *AIAA J.,* September 1982, pp. 1275-1281.
15. Coakley, T.J., and Huang, P.G.: "Turbulence Modeling for High Speed Flows," *AIAA-92-0436,* January 1992.
16. Huang, P.G., and Coakley, T.J.: "Turbulence Modeling for Complex Hypersonic Flows," to be presented *AIAA-93-0200,* January 1993.
17. Bardina, J.E.: "Turbulence Modeling for Hypersonic Flight," MCAT Inst., *PR 92-010, NASA-CR-190313,* May 1992.
18. Bardina, J., and Lombard C.K.: "Three Dimensional Hypersonic Flow Simulations with the Implicit Upwind Navier-Stokes Method," *AIAA-87-1114-CP,* 1987.
19. Bardina, J., and Lombard, C.K.: "CSCM Three Dimensional Navier-Stokes Computational Aerodynamics for a Projectile Configuration at Transonic Velocities," *AIAA-88-2585-CP,* 1988.
20. Chakravarthy, S. R.: "Relaxation Methods for Unfactored Implicit Upwind Schemes," *AIAA 84-0165,* 1984.
21. Wilcox, D.C.: "The Remarkable Ability of Turbulence Model Equations to Describe Transition," *AIAA-92-0000,* January 1992.
22. Horstman, C.C.: "Hypersonic Shock- Wave Turbulent-Boundary-Layer Interaction Flows - Experiment and Computation," *AIAA-91-1760,* June 1991.
23. Baldwin, B.S., and Lomax, H.: "Thin Layer Approximation and Algebraic Model for Separated Turbulent Flows," *AIAA-78-0257,* 1973.
24. Ames Research Staff: "it Equations, Tables and Charts for Compressible Flow," *NACA Report 1135,* 1953, p. 19.
25. Hopkins, E.J., and Inouye, M.: "An Evaluation of Theories for Predicting Turbulent Skin Friction and Heat Transfer on Flat Plates at Supersonic and Hypersonic Mach Numbers," *AIAA J.,* Vol. 9, No. 6, June 1971, pp. 993-1003.
26. Bradshaw, P.: "Compressible Turbulent Shear Layers," *Ann. Rev. of Fluid Mech.,* Vol. 9, 1977.)

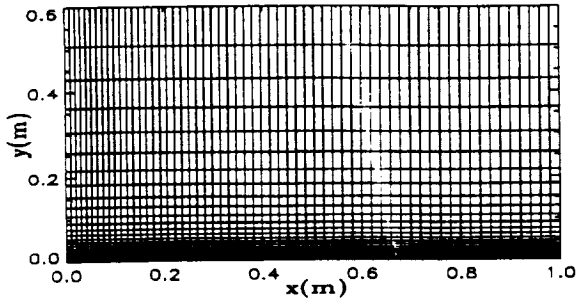

Figure 1a. 3x61x61 flat plate grid.

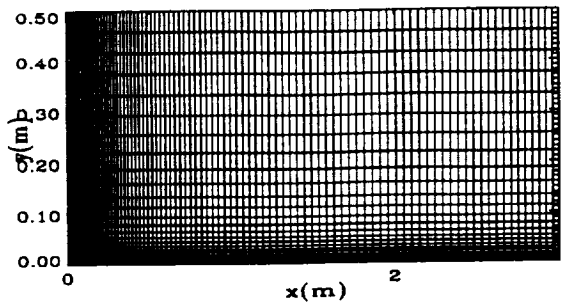

Figure 2a. 91x61x3 flat plate grid.

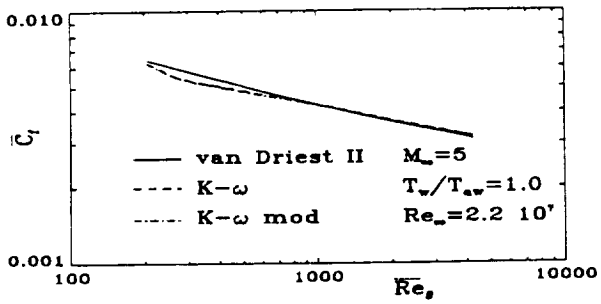

Figure 1b. Skin friction on insulated plate.

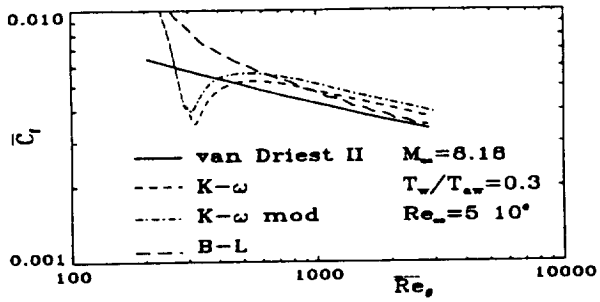

Figure 2b. Skin friction on cooled plate.

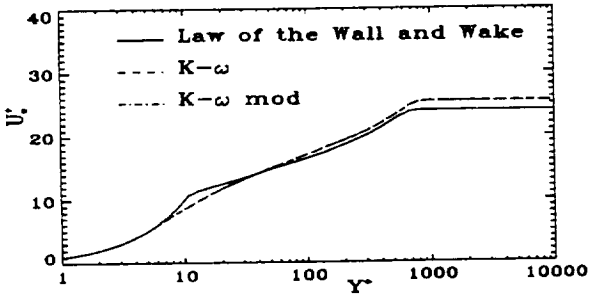

Figure 1c. Velocity profile on insulated plate.

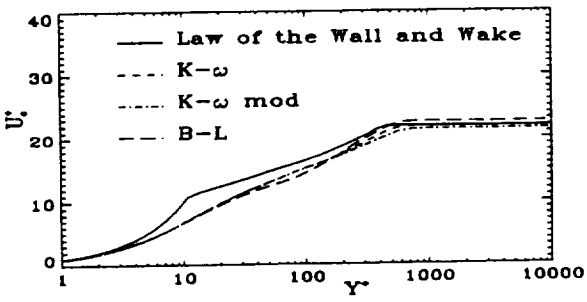

Figure 2c. Velocity profile on cooled plate.

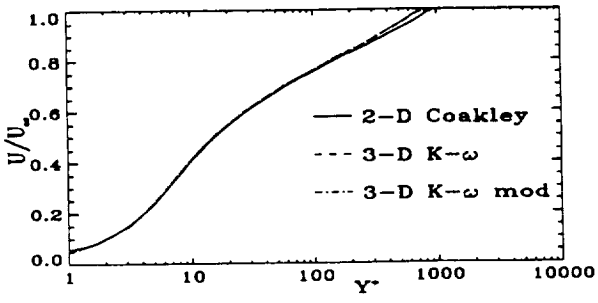

Figure 1d. Velocity profile on insulated plate.

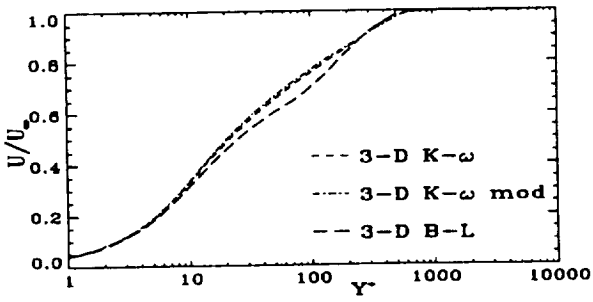

Figure 2d. Velocity profile on cooled plate.

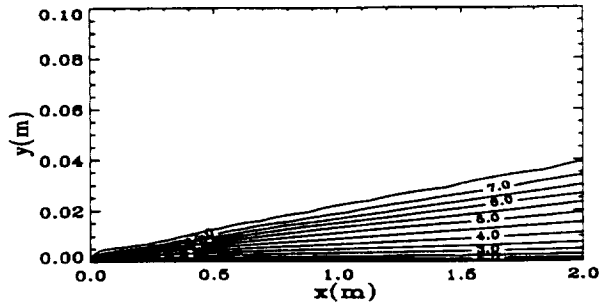

Figure 2e. Mach contour lines in cooled plate. k-w baseline model.

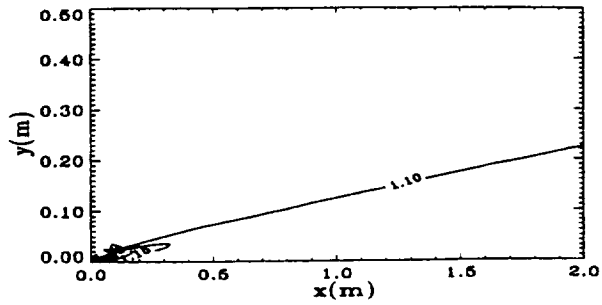

Figure 2f. Normalized pressure contours in cooled plate. k-w baseline model.

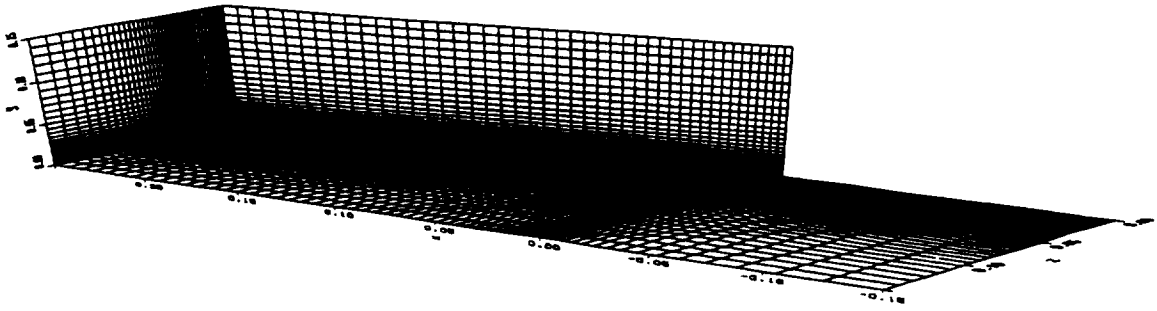

Figure 3. 61x41x61 SWBLI grid showing plate, fin ,and outflow planes.

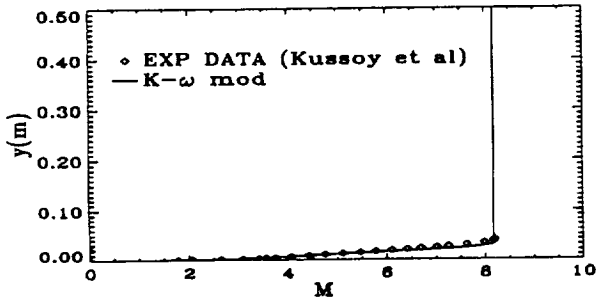

Figure 4a. Inflow SWBLI Mach profile.

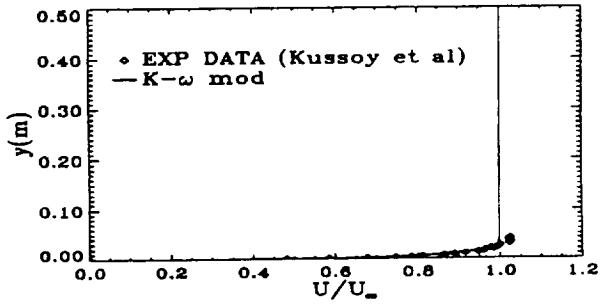

Figure 4b. Inflow SWBLI velocity profile.

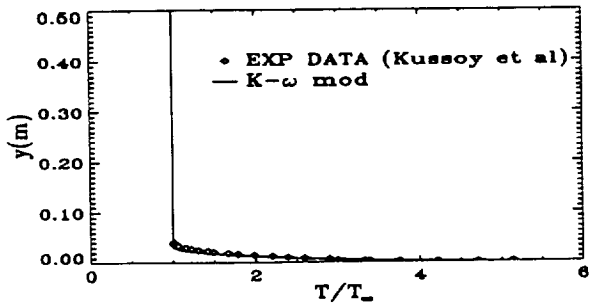

Figure 4c. Inflow SWBLI temperature profile.

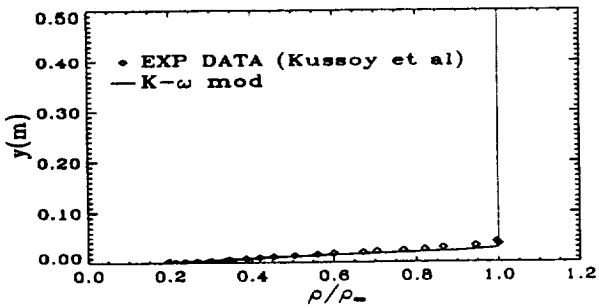

Figure 4d. Inflow SWBLI density profile.

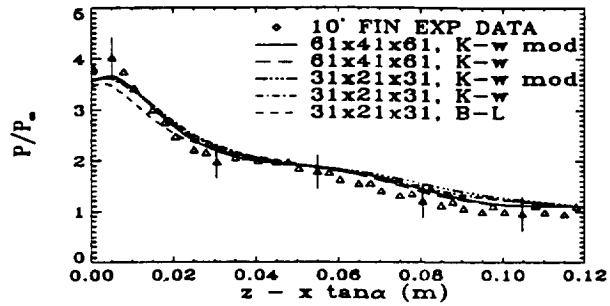

Figure 5a. Comparison of pressure profile on plate surface at x=0.1819 m.

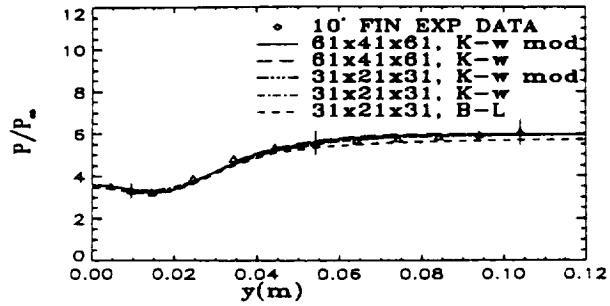

Figure 5b. Comparison of pressure profile on fin surface at s=0.1834 m from fin leading edge.

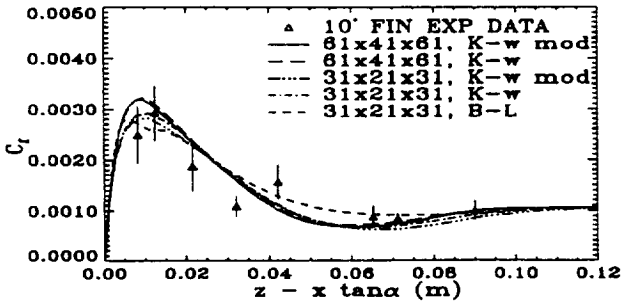

Figure 5c. Comparison of skin friction profile on plate surface at x=0.155 m.

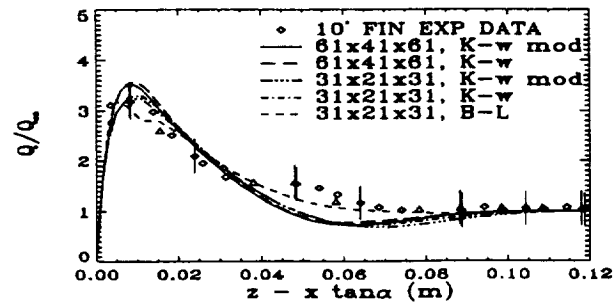

Figure 5d. Comparison of heat transfer rate profile on plate surface at x=0.1645 m.

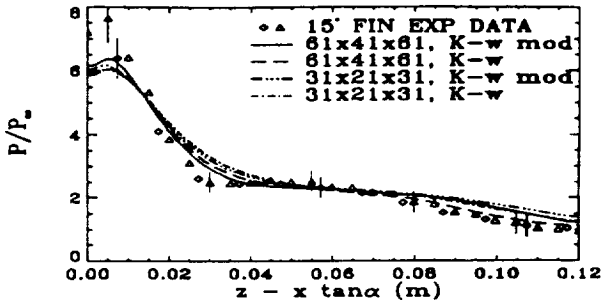

Figure 6a. Comparison of pressure profile on plate surface at x=0.1819 m.

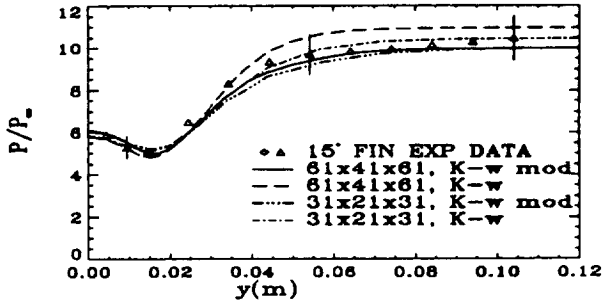

Figure 6b. Comparison of pressure profile on fin surface at s=0.1834 from fin leading edge.

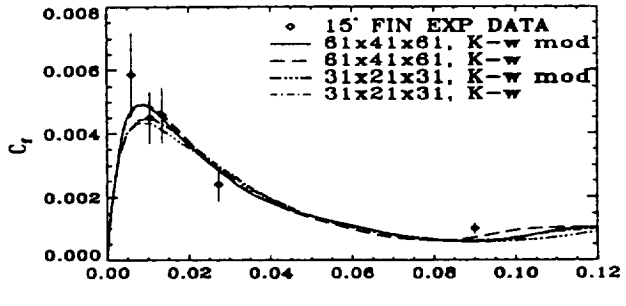

Figure 6c. Comparison of skin friction profile on plate surface at x=0.155 m.

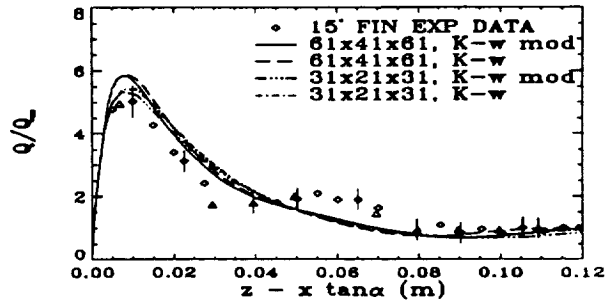

Figure 6d. Comparison of heat transfer rate profile on plate surface at x=0.1645 m.

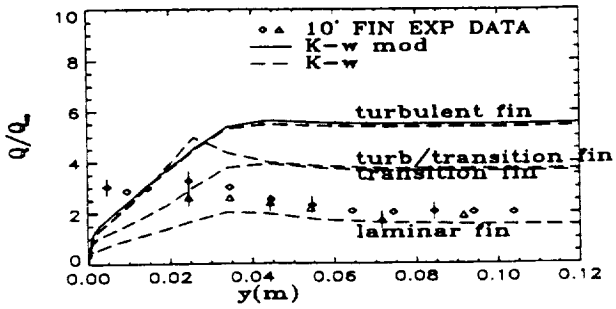

Figure 5e. Comparison of heat transfer rate profile on fin surface at s=0.167 m and s=0.1962 m with/without turbulence model on fin.

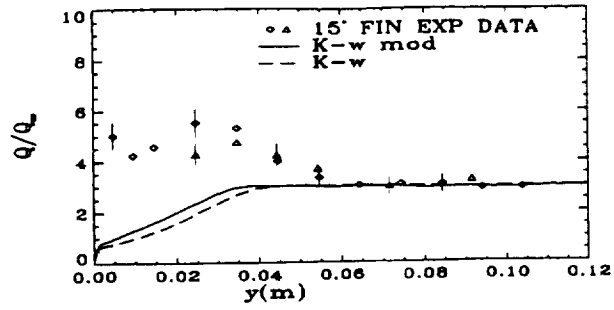

Figure 6e. Comparison of heat transfer rate profile on fin surface at s=0.167 m and s=0.1962 m without turbulence model on fin.

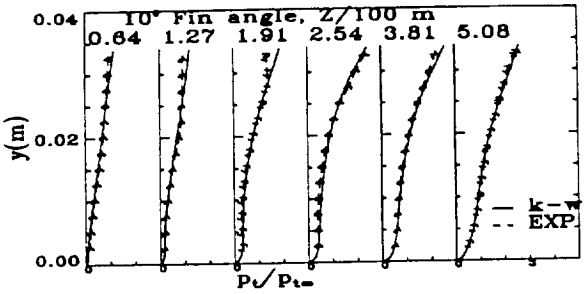

Figure 5f. Comparison of pitot pressure profiles at x=0.1723 m.

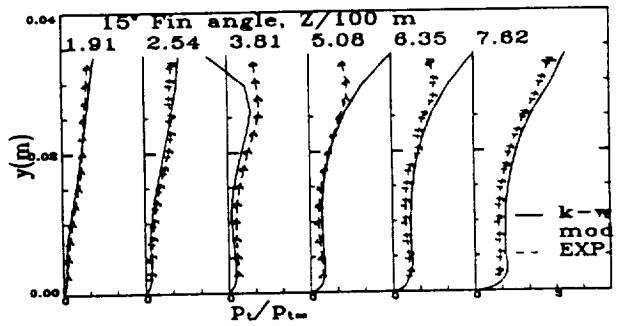

figure 6f. Comparison of pitot pressure profiles at x=0.1744 m.

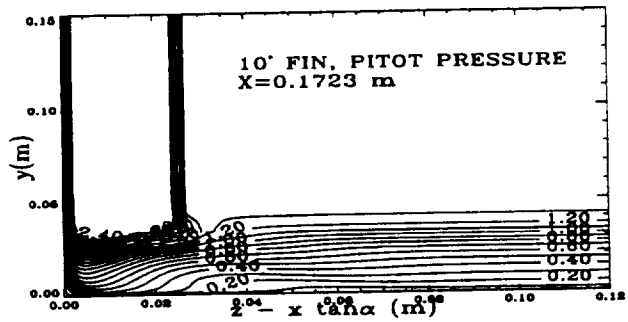

Figure 5g. Pitot pressure contours.

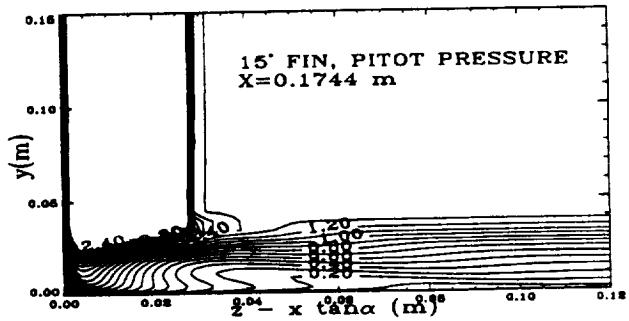

Figure 6g. Pitot pressure contours.

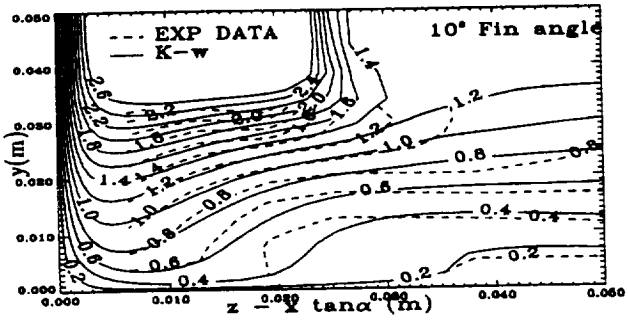

Figure 5h. Comparison of pitot pressure contours at x=0.1723 m.

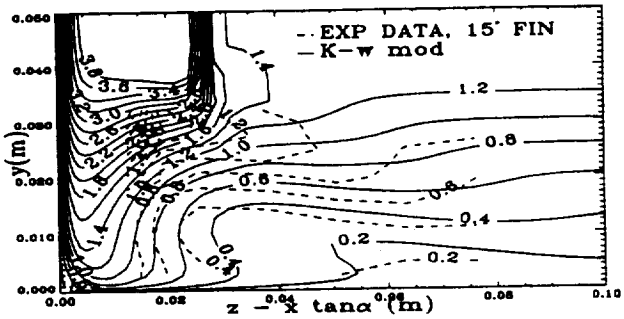

Figure 6h. Comparison of pitot pressure contours at x=0.1744 m.